Clim Dyn (2016) 47:3203–3220
DOI 10.1007/s00382-016-3021-y

Interdecadal modulation of ENSO-related spring rainfall over South China by the Pacific Decadal Oscillation

Xiaofei Wu[1,3] · **Jiangyu Mao**[1,2]

Received: 22 September 2015 / Accepted: 3 February 2016 / Published online: 11 February 2016

Abstract The interdecadal modulation of the relationship between El Niño–Southern Oscillation (ENSO) and the South China spring rainfall (SCSR) by the Pacific Decadal Oscillation (PDO) is investigated using long-term observational datasets. When ENSO and PDO are in-phase [i.e., El Niño events during warm PDO (EN_WPDO) and La Niña events during cold PDO (LN_CPDO)], the positive correlations between ENSO and SCSR are enhanced significantly, with above-normal (below-normal) SCSR generally following EN_WPDO (LN_CPDO) events. In contrast, the ENSO–SCSR relationship becomes ambiguous when ENSO and PDO are out-of-phase [i.e., El Niño events during cold PDO (EN_CPDO) and La Niña events during warm PDO (LN_WPDO)]. The PDO modulates the ENSO–SCSR relationship through the impact of variations in the lower-tropospheric subtropical anticyclone over the western North Pacific (WNP) and upper-tropospheric westerly jets over East Asia and the midlatitude North Pacific. An EN_WPDO (LN_CPDO) event induces an enhanced subtropical anticyclone (cyclone) over the WNP and intensified (weakened) subtropical westerly jet around the southern Tibetan Plateau due to modification by the PDO-forced anomalous circulation. Thus, South China falls just under the influence of the anomalous lower-tropospheric southwesterlies (northeasterlies) and upper-tropospheric divergent (convergent) environment, leading to above-normal (below-normal) SCSR. In contrast, the SCSR anomalies exhibit no wet or dry preference following EN_CPDO (LN_CPDO) events, because ENSO-induced and PDO-forced circulation anomalies tend to cancel each other out. These modulating effects by the PDO on the ENSO–SCSR relationship and related physical processes are also examined with coupled model simulations.

Keywords Interdecadal modulation · South China spring rainfall · ENSO · Pacific Decadal Oscillation · Coupled model simulation

✉ Jiangyu Mao
mjy@lasg.iap.ac.cn

[1] State Key Laboratory of Numerical Modeling for Atmospheric Sciences and Geophysical Fluid Dynamics (LASG), Institute of Atmospheric Physics, Chinese Academy of Sciences, P.O. Box 9804, Beijing 100029, China

[2] Joint Center for Global Change Studies, Beijing 100875, China

[3] University of Chinese Academy of Sciences, Beijing 100049, China

1 Introduction

Over eastern China and extratropical East Asia as a whole, the major rainy season is in summer (June–August, JJA), beginning approximately with the onset of the East Asian summer monsoon over the South China Sea around mid-May (Tao and Chen 1987; Mao et al. 2004). With the development of the prevailing monsoonal southwesterly and its extension northward, the Meiyu front is established over the Yangtze Basin around mid-June and heavy rainfall occurs over northern China in late July to early August (Lau and Li 1984; Tao and Chen 1987; Ding 2004). However, another significant rainy season exists in spring (March–May, MAM) over South China (SC, specifically south of the Yangtze Basin), known as the spring persistent rains (Wan and Wu 2009). Linho et al. (2008) noted that the rainfall in March and April accounts for one-quarter to one-third of the annual total near the mountainous border between Guangdong and Fujian provinces in SC. As shown in Fig. 1a, the MAM total rainfall exceeds 500 mm over

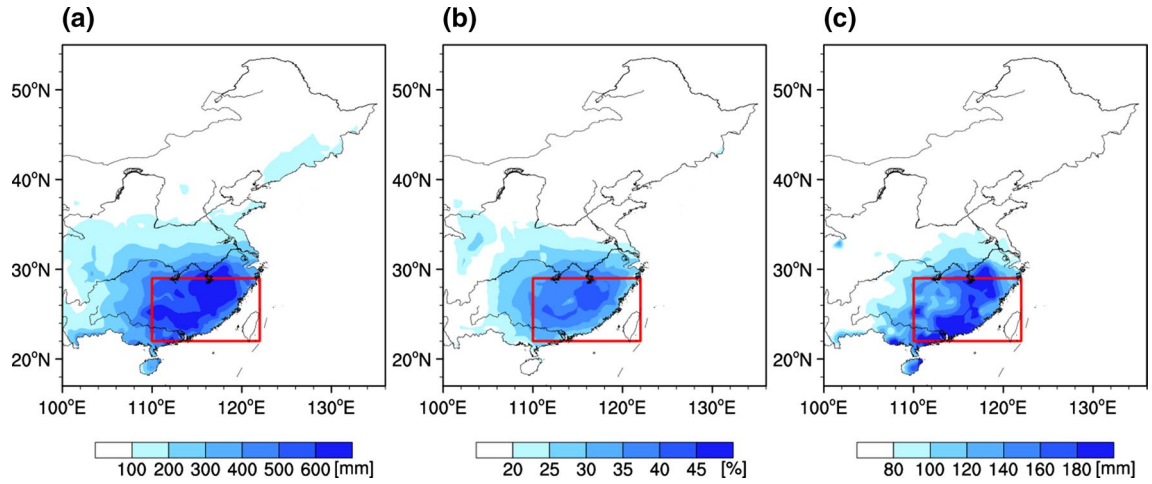

Fig. 1 Climatological distributions of boreal spring (March–May) **a** total rainfall (*color shading*, mm), **b** percentage of the annual total rainfall (*color shading*, %), and **c** interannual standard deviation (*color shading*, mm) over eastern China based on rain-gauge station data for the period 1951–2013. In (**a**) to (**c**), the *red rectangle* encloses most of South China

SC, contributing more than 35 % of the annual total rainfall over this region (Fig. 1b), approximately the same as the contribution of JJA rainfall to the annual total (Yang and Lau 2004). Thus, the South China spring rainfall (SCSR) is as important as the summer rainfall. Furthermore, the SCSR possesses strong interannual variability, with the standard deviation exceeding 140 mm (Fig. 1c), nearly 30 % of the MAM total rainfall. Associated with such strong interannual variability, severe floods and droughts occur frequently over SC during MAM, directly causing severe socioeconomic losses. Thus, it is of great importance to study the interannual variability of SCSR and explore the processes responsible for the large variations.

Previous studies suggested that the interannual variability in SCSR is influenced by climatic factors from the mid-high latitudes and the tropics (Wu and Kirtman 2007; Feng and Li 2011; Shao and Zhang 2012; Zheng and Li 2012; Chen et al. 2013a, b). Shao and Zhang (2012) noted that above-normal (below-normal) SCSR is usually preceded by a positive (negative) phase of the North Atlantic Oscillation. A similar positive relationship exists between SCSR and western Siberian spring snow cover (Wu and Kirtman 2007). Both the North Atlantic Oscillation and the western Siberian spring snow cover can affect SCSR through a wave pattern over the eastern Atlantic through Europe and midlatitude Asia (Wu and Kirtman 2007; Shao and Zhang 2012). The midlatitude circulation anomalies in the Southern Hemisphere may also influence SCSR. For instance, the preceding winter Southern Hemisphere Annular Mode may impact the SCSR via sea surface temperature (SST) anomalies in mid-high latitudes in the Southern Hemisphere as a manifestation of the "ocean–atmosphere coupled bridge" (Zheng and Li 2012; Zheng et al. 2015). Other studies have also shown that the distribution of SST anomalies (SSTAs) is an important factor for the interannual variability of SCSR, especially in the Pacific (Deng and Wang 2002; Wu et al. 2003; Feng and Li 2011; Qiang and Yang 2013). Thus, the relationship between SCSR and interannual–interdecadal variations in Pacific SSTs requires further study.

As the most dominant variability in air–sea interaction on interannual timescales, the El Niño–Southern Oscillation (ENSO) has tremendous impacts on both summer rainfall (Huang and Wu 1989; Tao and Zhang 1998; Karori et al. 2013) and winter rainfall (Tao and Zhang 1998; Zhou and Wu 2010; Zhou et al. 2010) in East Asia. The key system that links the eastern tropical Pacific warm (cold) SSTAs during El Niño (La Niña) events and rainfall anomalies over East Asia is an anomalous lower-tropospheric anticyclone (cyclone) located in the western North Pacific (WNP) (Wang et al. 2000). However, the impacts of ENSO on SCSR have received little attention. In investigating seasonal rainfall anomalies in East Asia during different phases of ENSO, Wu et al. (2003) suggested that a weak positive relationship exists between ENSO and SCSR during the decaying phases of ENSO. Similar results have shown that the relationship between ENSO and rainfall over eastern China is weakest in spring and that the relationship experienced a decadal change around the 1970s (Gao et al. 2006). Since the late 1970s, the frequency of ENSO Modoki events has clearly been increasing (Ashok et al. 2007). Feng and Li (2011) demonstrated that typical El Niño and El Niño Modoki events influence SCSR differently, with the El Niño Modoki leading to a below-normal SCSR and the typical El Niño resulting in an above-normal SCSR. However, Gong and Wang (1998) investigated the

relationship between ENSO and seasonal rainfall in China based on a longer time series from 1880 and found no statistically significant connection between ENSO and SCSR. These results indicate that interdecadal changes may exist in the SCSR–ENSO relationship.

Indeed, some studies have shown that the impacts of ENSO on climate are not stationary and could be modulated by the Pacific Decadal Oscillation (PDO; Mantua et al. 1997; Gershunov and Barnett 1998; Zhu and Yang 2003; Chan and Zhou 2005; Mao et al. 2011; Feng et al. 2014; Kim et al. 2014; Wang et al. 2014). The PDO may modulate the ENSO-related tropical atmospheric circulation, especially the spatial pattern and strength of the ENSO-related anticyclone over the WNP. Wang et al. (2008) suggested that the anomalous anticyclone displays notable differences between warm and cold phases of the PDO, with the anticyclone being confined south of the Philippines (shifting northward to the east of the Philippines) during the warm (cold) phases of the PDO. Furthermore, Kim et al. (2014) demonstrated that the negative relationship between ENSO and the East Asian winter monsoon is significant only when the ENSO and PDO are in-phase (i.e., El Niño–warm PDO events and La Niña–cold PDO events), because the WNP anticyclone expands greatly in El Niño–warm PDO combinations but dramatically shrinks in La Niña–cold PDO combinations. A similar modulating effect also exists during the early summer (May–June), with monsoon rainfall anomalies over SC being significantly below or above normal more often when ENSO and PDO are in-phase, whereas no anomalous dry or wet preference is apparent when they are out-of-phase (Chan and Zhou 2005). Under the different PDO backgrounds, the evolution of ENSO-related SST anomalies shows significantly different characteristics, which further influences the WNP subtropical high and the East Asian monsoon rainfall (Chen et al. 2013b; Lee et al. 2013). Alternatively, the PDO may modulate the midlatitude teleconnection forced by ENSO (Gershunov and Barnett 1998; Yu and Zwiers 2007; Yoon and Yeh 2010). For example, when El Niño and PDO are in-phase (out-of-phase), the midlatitude Eurasian-like pattern acts to enhance (reduce) the summer rainfall over northeast Asia (Yoon and Yeh 2010). Chen et al. (2013a) found that the relationship between SC winter–spring precipitation and ENSO exhibits interdecadal changes, and suggested that such changes are related to increased SST variability in the eastern South Indian Ocean and modulation of the PDO. Because the East Asian monsoon exhibits multiscale variations, in which intraseasonal oscillations are an important variability in determining active and break sequences within each summer or winter monsoon season (e.g., Tao and Chen 1987; Ha et al. 2012), ENSO may lead to seasonal-mean rainfall anomalies of the East Asian monsoon through affecting the intraseasonal behaviors (Yun et al. 2010; Ha et al. 2012). As suggested by Ha et al. (2012), the intraseasonal variability in EASM plays a more important role in the explanations of the interannual variability and climate change than does the annual mean. Yun et al. (2010) noticed that the relationship between ENSO and northward-propagating intraseasonal oscillation (NPISO) shows a decadal change, with the preceding winter ENSO influencing the early summer (May to June) NPISO through ENSO-induced West Pacific pattern before the late 1970s and the later summer (July to August) NPISO through Pacific-Japan pattern after the late 1970s. The maximum rainfall over the Korean Peninsula also shows a decadal shift from July to August after the mid-1970s, resulting from the changes of the relationship between August rainfall and ENSO (Lee et al. 2010). But how does the PDO modulate the SCSR–ENSO relationship? Given that both ENSO and PDO are the dominant sources of predictability of interannual and interdecadal climate variability, revealing the physical mechanism for the PDO modulation of the SCSR–ENSO relationship is of high value for improving seasonal predictions of SCSR.

In this context, the objective of the present study is to explore the impact of ENSO on interannual variability of SCSR under different PDO backgrounds, thereby understanding the physical mechanism by which the PDO modulates the ENSO–SCSR relationship. Section 2 presents the data and methods used in this study. In Sect. 3, we investigate the respective impacts of the PDO and ENSO on the SCSR. The ENSO-related SCSR anomalies under different PDO backgrounds and the physical mechanism for the PDO modification of the ENSO–SCSR relationship are presented in Sect. 4. The findings are then verified by examined in numerical simulation, as reported in Sect. 5. Finally, Sect. 6 presents a summary of the results.

2 Data and methods

2.1 Observations and reanalysis data

Because the present study focuses on the interdecadal modulation of ENSO-related SCSR by the PDO, it is necessary to utilize observational and reanalysis datasets over as long a period as possible. Long-term gridded rainfall records are available from the Climate Research Unit (CRU) Time-Series (TS) version 3.22, covering the period 1901–2013, with a high spatial resolution of 0.5° latitude × 0.5° longitude (Harris et al. 2014). The CRU TS3.22 dataset is constructed from monthly observations at meteorological stations across the world's land areas, with extensive manual and semi-automated quality control measures. Monthly rain-gauge precipitation datasets since 1951 at 160 Chinese meteorological stations, provided by the China

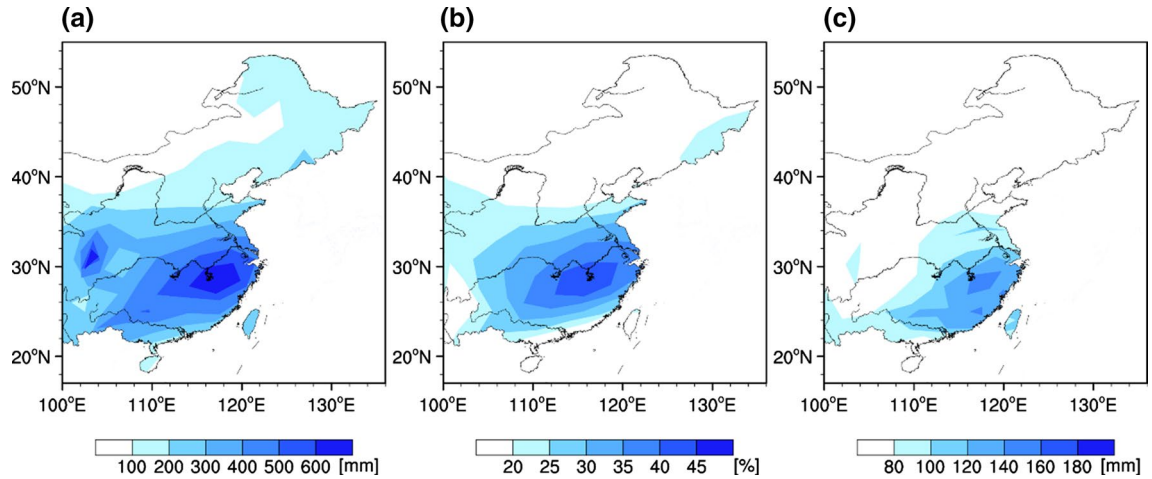

Fig. 2 As for Fig. 1 except for simulated rainfall from the CCSM4 CMIP5 historical run for the period 1951–2005

Meteorological Administration, are also used to verify the reliability of the CRU TS 3.22 reanalysis rainfall.

Monthly SST data for the period 1920–2013 are extracted from the UK Met Office Hadley Centre Sea Ice and SST dataset version 1.1 (HadISST 1.1). The HadISST replaces the Global Sea Ice and Sea Surface Temperature (GISST) dataset, and is a unique combination of monthly globally complete fields of SST and sea ice concentration on a 1° × 1° latitude–longitude grid from 1870 to the present (Rayner et al. 2003). To ensure the consistency of the PDO and ENSO, the PDO and Nino3.4 indices are recalculated using the HadISST 1.1 (see Sect. 2.3).

The twentieth century atmospheric reanalysis (ERA-20C) products are analyzed to demonstrate the ENSO-related anomalous teleconnection patterns under recent warm and cold PDO epochs. These data are provided by the European Centre for Medium-Range Weather Forecasts (ECMWF) and are currently available for the period 1901–2010 (Stickler et al. 2014). Although there is another reanalysis product covering the entire twentieth century, the twentieth century reanalysis version 2 (20CR V2; Compo et al. 2011) from the National Oceanic and Atmospheric Administration–Cooperative Institute for Research in Environmental Sciences (NOAA–CIRES), it differs from ERA-20C in terms of assimilated surface observations. The boundary SST and surface pressure datasets assimilated in ERA–20C are HadISST version 2.1, the International Surface Pressure Databank (ISPD) version 3.2.6, and the International Comprehensive Ocean–Atmosphere Data Set (ICOADS) version 2.5.1, whereas 20CR V2 only uses the earlier versions of these data (namely HadISST v1.1, ISPD v2, and ICOADS v2.4). This is first reason to utilize the ERA-20C rather than 20CR V2 products. Another reason for using ERA-20C is its higher horizontal resolution with a ~125 km (spectral truncation T159) latitude–longitude grid and vertical resolution with 37 levels from 1000 to 1 hPa, because the higher resolution reanalysis can reproduce more realistic spring rainfall pattern over SC (Li et al. 2015).

2.2 Simulation data

The "twentieth century" simulations forced by observed atmospheric composition changes (reflecting both anthropogenic and natural sources) from the Coupled Model Intercomparison Project Phase 5 (CMIP5) offer opportunities to understand air–sea interactions and atmospheric responses to SST anomalies at regional and global scales (Taylor et al. 2012). As evaluated by Sperber et al. (2013), of the 25 CMIP5 coupled general circulation model simulations for the late twentieth century climate, those derived from the Community Climate System Model (version 4, CCSM4) perform well in simulating both the climatology and interannual variability of the boreal Asian summer monsoon, including precipitation and lower-tropospheric circulation. The CCSM4 also performs well in reproducing the spatial pattern and temporal evolution of the PDO and ENSO (DeFlorio et al. 2013). Thus, Krishnamurthy and Krishnamurthy (2014) used CCSM4 simulations to study the influence of the PDO on the South Asian summer monsoon–ENSO relation. More importantly, CCSM4 also has a reasonable representation of the climatology and interannual variability of SCSR. The distribution of the CCSM4-simulated climatological spring rainfall over eastern China (Fig. 2a) shows heavy rainfall (>500 mm) mostly over SC, bearing some resemblance to the observational distribution (Fig. 1a), although the simulated rainfall amount is somewhat underestimated over the coastal area, and the belt of heavy rainfall extends slightly northward into the Yangtze Basin. The simulated percentage of spring rainfall

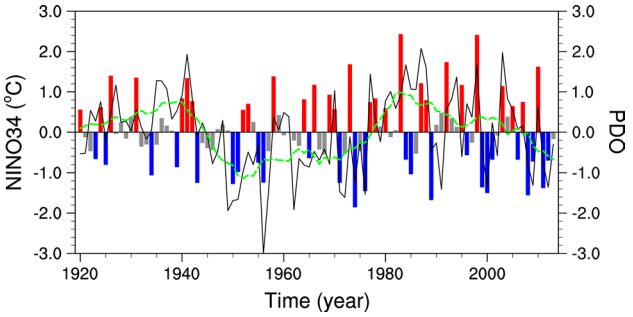

Fig. 3 Detrended Nino3.4 index (*bars*) and normalized PDO index (*black line*) averaged for December–February (DJF) for the period 1920–2013. The *green dashed line* represents the decadal-scale fluctuations of the PDO index as indicated by the 11-year running mean (the reflective condition is utilized to calculate the start and end points of running mean). *Red* and *blue bars* denote El Niño and La Niña years, respectively

relative to annual total (Fig. 2b) is also similar to observations (Fig. 1b). Furthermore, the region of large interannual standard deviation (Fig. 2c) of the CCSM4-simulated rainfall concentrated mostly over SC is also consistent with observations (Fig. 1c). Thus, the CCSM4 CMIP5 historical simulations are used to validate the physical mechanism for the PDO modulation of the ENSO–SCSR relationship in Sect. 5.

2.3 Analysis methods

The PDO index used in this study is reconstructed according to the definition given by Mantua et al. (1997). For this purpose, an empirical orthogonal function (EOF) analysis is performed on detrended monthly SST anomalies over the domain 20°–60°N, 120°E–120°W for the period 1920–2013. The data are detrended by subtracting the globally averaged SST anomalies. The normalized principle component (PC1) is defined as the monthly mean PDO index. In this study, we focus on the winter (December–February, DJF) averaged PDO index (defined as the average of the DJF monthly means), as shown in Fig. 3. The 11-year running mean of the DJF-averaged PDO index is used to represent the interdecadal variability of the PDO, which exhibits two positive epochs (1921–1945 and 1978–2006) and two negative epochs (1946–1977 and 2007–2013) (Fig. 3). Because most ENSO events tend to reach their peak in winter months, in this study ENSO events are defined to occur when the detrended DJF Nino 3.4 SST anomalies are more than 0.6 standard deviations (0.6σ is approximately equal to 0.55 °C) away from the long-term mean. The detrended Nino3.4 index is employed to avoid the possible influence of phase shifts in the PDO (Gershunov and Barnett 1998). Following this definition, 26 El Niño winters and 26 La Niña winters are identified for the period 1922–2013. As the interannual variability of the Nino3.4 index is modulated by interdecadal fluctuations of the PDO (Fig. 3), these ENSO events are classified into four categories based on whether they are in warm or cold PDO epochs (Table 1). For convenience, an El Niño event occurring in a warm PDO epoch is represented as El Niño–warm PDO (EN_WPDO). Similarly, other categories are denoted as El Niño–cold PDO (EN_CPDO), La Niña–warm PDO (LN_WPDO), and La Niña–cold PDO (LN_CPDO). The ENSO events and different ENSO-PDO combinations are defined based on the Niño3.4 SST index averaged over the winter months (DJF) when an ENSO event typically matures. The influences of these events on rainfall anomalies during the subsequent spring, i.e., when ENSO decays, are then examined. Unless otherwise stated, ENSO-related circulation and rainfall anomalies in the following text refer to those in the spring following the peak of ENSO events. To demonstrate the ENSO-related circulation anomalies associated with anomalous SCSR under different PDO backgrounds, composite and sub-composite analyses are performed for the four ENSO categories. The statistical significance of the composite differences is estimated through bootstrap resampling (Efron 1982; Gershunov and Barnett 1998). Bootstrap resampling is a nonparametric statistical method that is superior to other statistical test methods in terms of its being applicable to both small and large sample sizes. The composite difference at each grid is computed repeatedly 5000 times using the resampled variable series derived from random permutations of the original series. The 0.025th and 0.975th quantiles are the lower and upper bounds of the bootstrapped 95 % confidence interval.

Table 1 El Niño or La Niña years sorted by PDO phase for the period 1922–2013

	Warm PDO	Cold PDO
El Niño	1924, 1926, 1931, 1940, 1941, 1942, 1978,1980, 1983, 1987, 1988, 1992, 1998, 2003, 2005	1952, 1953, 1958, 1964, 1966, 1969, 1970, 1973, 1977, 2007, 2010
La Niña	1923, 1925, 1934, 1939, 1943, 1984, 1985, 1989, 1996, 1999, 2000, 2001, 2006	1950, 1951, 1955, 1956, 1965, 1968, 1971, 1974, 1976, 2008, 2009, 2011, 2012

A calendar year such as 1924 refers to the 1923/1924 El Niño event

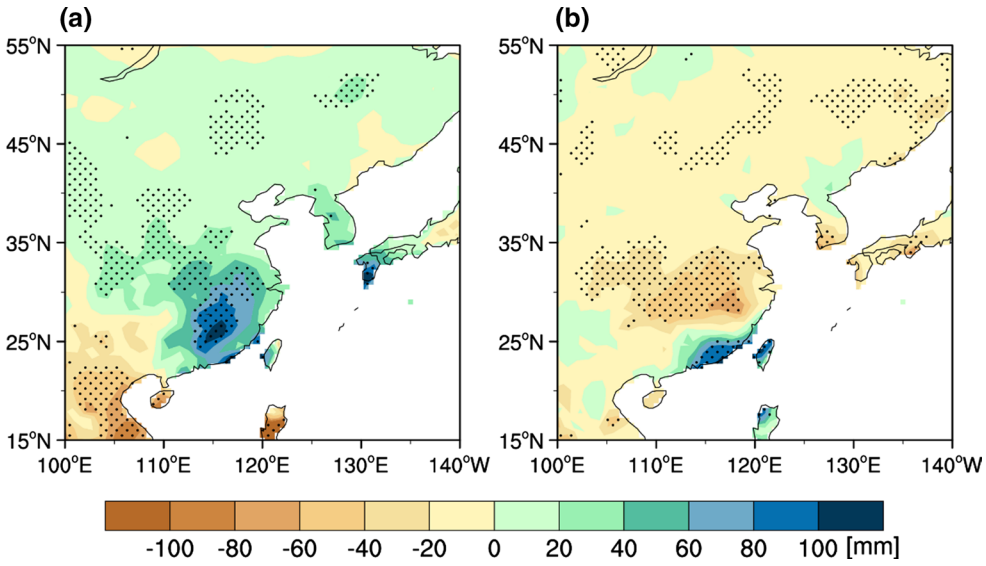

Fig. 4 Composite differences of spring (March–May) total rainfall (*color shading*, mm) **a** between El Niño and La Niña years and **b** between warm PDO and cold PDO epochs. The *stippling* denotes statistical significance at the 95 % confidence level

3 Respective impacts of the PDO and ENSO on SCSR

Before exploring the interdecadal modulating effect of the PDO on the ENSO–SCSR relationship, the impacts on SCSR of each of the PDO and ENSO are first examined in turn in this section. Composite differences (Fig. 4a) between El Niño and La Niña years show that the following spring rainfall tends to be above-normal over most of East Asia, but below-normal over southwestern China and the Indo-China Peninsula. Note that the larger positive rainfall anomalies in southeastern China just north of 25°N are significant, but those over the SC coastal region are not, which is consistent with previous results (Wu et al. 2003). However, the composite differences (Fig. 4b) between warm and cold PDO epochs demonstrate that the spring rainfall tends to be below-normal over East Asia during warm PDO epochs but with significant positive rainfall anomalies around the SC coastal region, almost the opposite of the rainfall anomaly pattern shown in Fig. 4a. This suggests that both the PDO and ENSO indeed exert significant impacts on the spring rainfall anomalies over eastern China, with a greater prevalence of positive anomalies over eastern China in El Niño years than in warm PDO years. Note that over SC where the same positive rainfall anomalies occur, the anomalies are more significant in warm PDO years than in El Niño years, indicating the dominant impact of the PDO on SCSR. It can be speculated that the significant positive rainfall anomalies over SC would be enhanced and extend northward if an El Niño event arose in the warm PDO epoch, while enhanced negative rainfall anomalies would be associated with a La Niña event occurring in cold PDO epochs, as discussed later.

Such different rainfall anomaly patterns are actually induced by the different circulation anomalies related to ENSO and PDO. In the spring following the ENSO mature phase, the SSTA pattern retains typical features of El Niño, with strong positive SSTAs over the central and eastern equatorial Pacific and weak negative SSTAs over the central North Pacific (Fig. 5a). As a response to the El Niño-related SSTAs, strong positive sea level pressure (SLP) anomalies occur over the western tropical Pacific and WNP, extending northward along the coast of East Asia (Fig. 5b), in association with a massive anomalous anticyclone covering both the tropics and mid-latitudes from the western to central North Pacific, extending to nearly 45°N and 170°W (Fig. 5c). Such an anomalous anticyclone results from a Rossby-wave response to the suppression of convective heating, which is induced by both in situ ocean cooling and subsidence forced remotely by central Pacific warming (Wang et al. 2000). Furthermore, the northward-extending anticyclonic anomalies force anomalous southwesterlies over East Asia (Fig. 5c), favoring above-normal rainfall over most regions of East Asia including SC and central China. In comparison with ENSO-induced SLP anomalies, the PDO-related positive SLP anomalies are only observed over the western tropical Pacific south of 20°N (Fig. 5f), associated with zonal anticyclonic anomalies extending from the WNP eastward to 150°W in the lower troposphere (Fig. 5f). Note that significant negative SLP anomalies exist over the North Pacific, extending southwestward to East Asia (Fig. 5f). Such an anomalous SLP pattern is a typical feature of the PDO, characterized by a negative SLP anomaly in the central North Pacific and a deepened Aleutian low (Mantua et al. 1997). Thus, a dipole-like anomalous circulation pattern with an anomalous zonally elongated anticyclone in the subtropical Pacific and

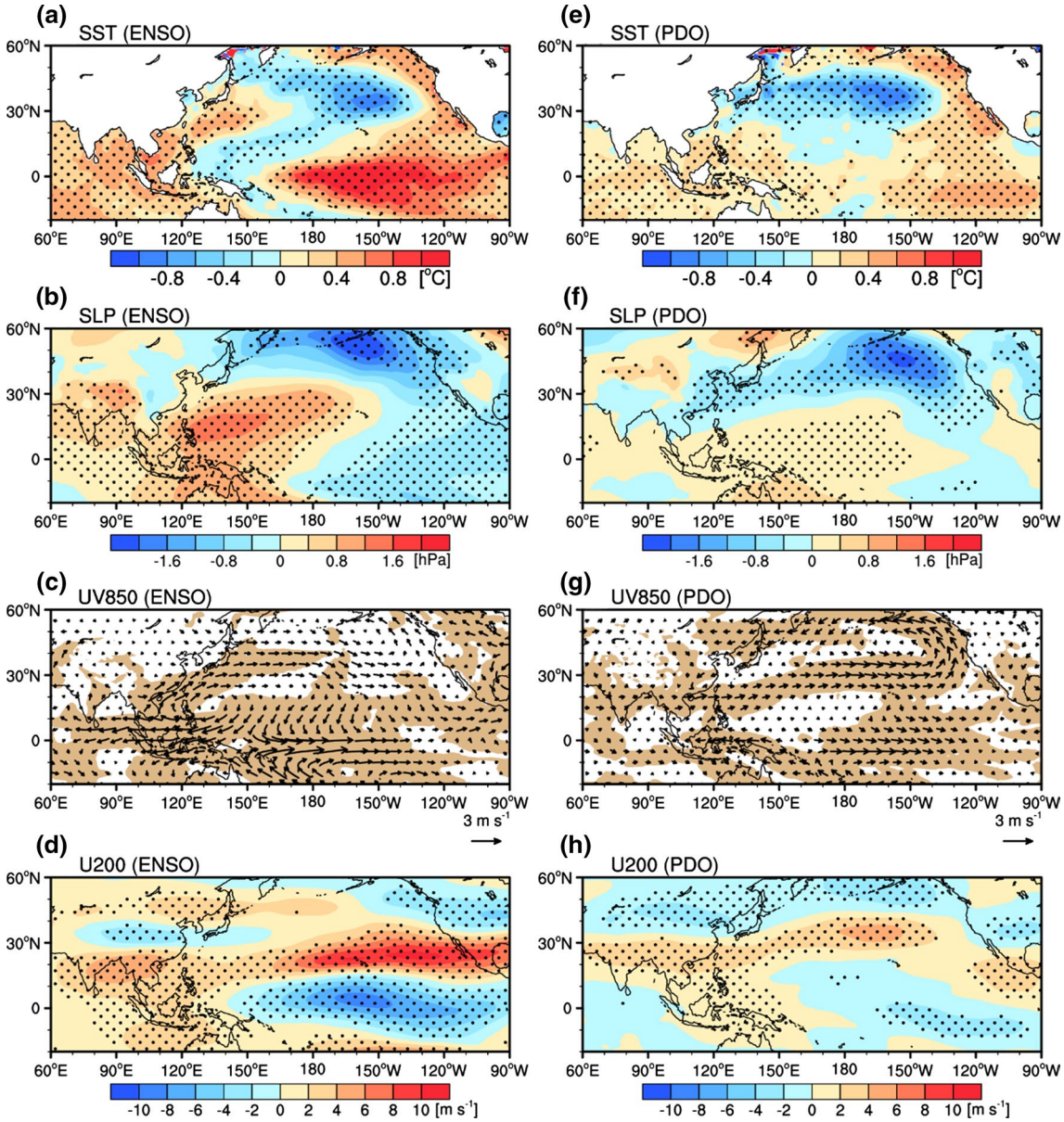

Fig. 5 Composite differences between (*left panels*) El Niño and La Niña years in spring (March–May) for **a** SST (*color shading*, °C), **b** SLP (*color shading*, hPa), **c** 850-hPa horizontal winds (*vectors*, m s^{-1}), and **d** 200-hPa zonal winds (*color shading*, m s^{-1}). *Right panels* (**e**) to (**h**) are as in (**a**) to (**d**), but for the composite differences between warm PDO and cold PDO epochs. The stippling in (**a**), (**b**), (**d**–**f**), and (**h**) denotes statistical significance at the 95 % confidence level, while the *shading* in (**c**) and (**g**) indicates the areas where at least one of the anomalous zonal and meridional wind components is statistically significant at the 95 % confidence level

an anomalous cyclone over the North Pacific dominates the subtropical and northern Pacific (Fig. 5g). As a result, the anomalous southwesterlies resulting from the subtropical anticyclone and the northerlies from the midlatitude cyclone converge over SC, leading to above-normal SCSR. However, the anomalous northeasterlies prevail over most of the East Asian regions north of SC, resulting in below-normal spring rainfall over these regions. In the upper-troposphere, both the ENSO and PDO are accompanied by a strengthened East Asian subtropical jet, though the jet anomaly forced by ENSO is stronger than that forced by the PDO (Fig. 5d, h). The strengthening of the subtropical jet can enhance the upper-tropospheric divergence over SC, contributing to the above-normal SCSR.

Note that since ENSO is modulated by the PDO (Fig. 3), the interannual SCSR anomalies associated with a given ENSO event may actually result from a synthesis of the effects caused by a particular ENSO–PDO combination. That is, the anomalous SCSR resulting from the ENSO-induced strong anomalous WNP anticyclone or cyclone

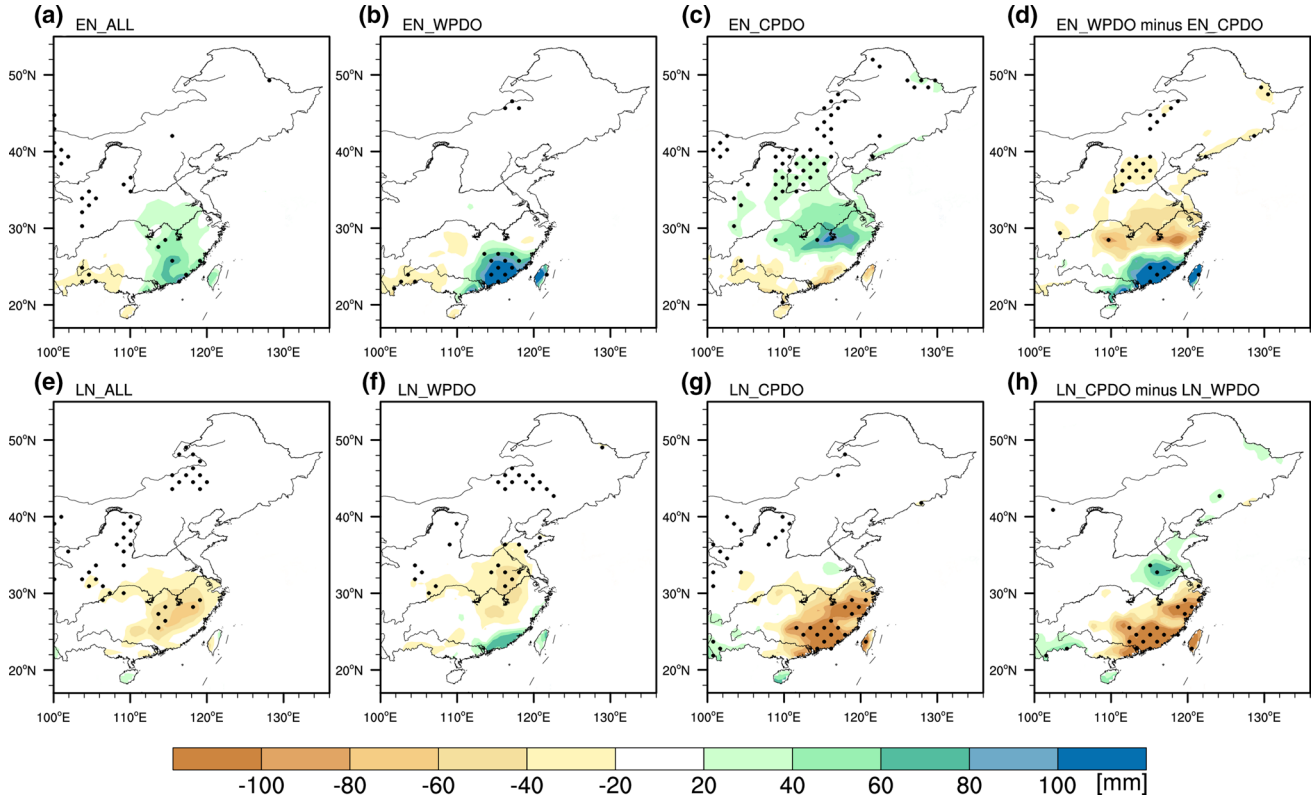

Fig. 6 Composite distributions of the spring (March–May) detrended rainfall (*color shading*, mm) in the period 1922–2013 for **a** all El Niño events (EN_ALL), **b** El Niño–warm PDO events (EN_WPDO), and **c** El Niño–cold PDO events (EN_CPDO). **d** Difference between ENSO in-phase and out-of-phase with PDO; i.e., (**b**) minus (**c**). The lower panels (**e**)–(**h**) are the corresponding distributions for La Niña events. *Stippling* denotes statistical significance at the 95 % confidence level

and subtropical jet over East Asia, may be modified by the somewhat different PDO-induced anomalous circulation, which is therefore examined in the next section.

4 PDO modulation of ENSO-related SCSR

4.1 Rainfall anomalies

As shown in Table 1, 26 El Niño events occurred during the period 1922–2013, comprising 15 El Niño–warm PDO events and 11 El Niño–cold PDO events. To demonstrate how the PDO modifies the relationship between ENSO and SCSR, Fig. 6a–d show the MAM rainfall anomalies over eastern China for the El Niño composite and the sub-composites according to the PDO phase, together with the difference between in-phase and out-of-phase combinations. If all 26 events are considered with no reference to PDO–ENSO combination, the El Niño-related rainfall shows above-normal amounts over East China, but this is barely significant at the 95 % confidence level (Fig. 6a). When the PDO epoch is considered, significant differences are observed between the spatial distributions of El Niño-related rainfall under warm and cold PDO epochs. During warm PDO epochs, significant positive rainfall anomalies occur over SC (Fig. 6b) that are much stronger than those without considering the PDO backgrounds (Fig. 6a). In contrast, El Niño–cold PDO events produce positive rainfall anomalies over the Yangtze basin and North China (Fig. 6c), with somewhat negative anomalies over SC, although they are insignificant at the 95 % confidence level (Fig. 6c). In addition, the El Niño-related rainfall differences between warm and cold PDO epochs (Fig. 6d) show significant positive rainfall anomalies over SC, with less significant negative anomalies over the Yangtze Basin and North China. The situation is reversed in the springs following La Niña events, for all La Niña cases, La Niña–warm PDO, La Niña–cold PDO combinations, and the composite difference between La Niña–cold PDO and La Niña–warm PDO (Fig. 6e–h). Note that the significant negative anomalies cover a much larger area over SC in the in-phase combination of La Niña with cold PDO (Fig. 6g) than the area covered by significant positive anomalies in the in-phase combination of El Niño with warm PDO (Fig. 6b).

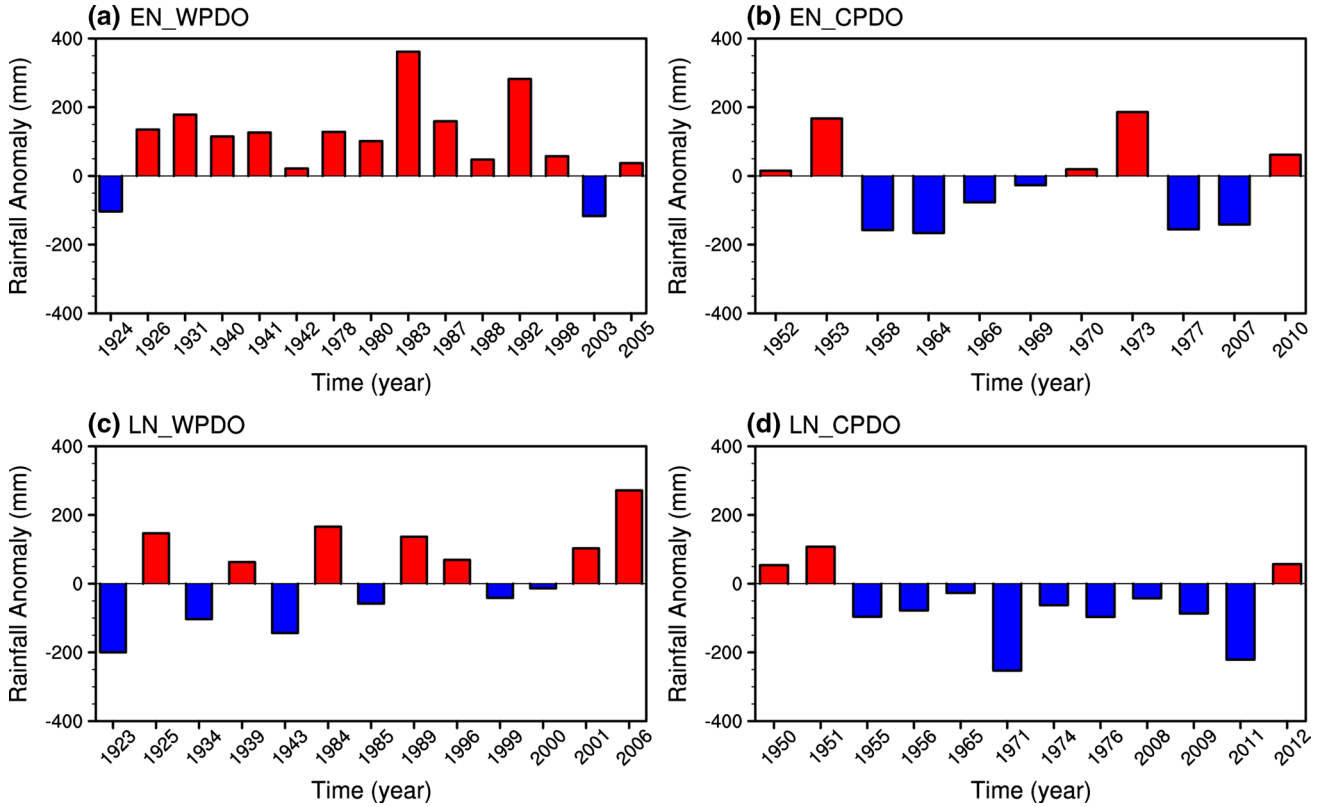

Fig. 7 Time series of the SCSR index for different combinations of PDO and ENSO events. **a** El Niño–warm PDO, **b** El Niño–cold PDO, **c** La Niña–warm PDO, and **d** La Niña–cold PDO. The *red* and *blue bars* denote positive and negative values, respectively. The SCSR index is defined as the area-averaged spring rainfall anomalies over SC (as shown by the *red rectangle* in Fig. 1). Anomalies are calculated as departures from the long-term mean for the period 1922–2013

These comparisons of the four sub-composites demonstrate that the PDO indeed plays an important role in modulating the ENSO–SCSR relationship. When ENSO and PDO are in-phase, the positive ENSO–SCSR relationship becomes much stronger, with above-normal SCSR following El Niño–warm PDO events and below-normal SCSR following La Nina–cold PDO events. The modulating effect can be further confirmed by examining year-by-year variations of the SCSR index. The SCSR index is defined as the area-averaged MAM total rainfall anomaly over SC (red rectangle in Fig. 1). The SCSR indices are shown separately in Fig. 7 for the four classified groups. When ENSO and PDO are in-phase, the SCSR index exhibits positive anomalies for 13 of the 15 El Niño–warm PDO years (Fig. 7a), and negative anomalies for 9 of the 12 La Niña–cold PDO years (Fig. 7d), corresponding to 75 % of the in-phase combinations. No significant preference of anomalous SCSR is evident when ENSO and PDO are out-of-phase (Fig. 7b, c).

4.2 SST and circulation anomalies

To explore the physical mechanism by which the PDO modulates the ENSO–SCSR relationship, the ENSO-related anomalous circulation is examined separately under warm and cold PDO epochs. Firstly, we analyze the El Niño-related circulation anomalies under different PDO backgrounds. As shown in Fig. 5 and suggested by previous studies, although the PDO and ENSO have similar SSTA patterns, the strong SSTAs in the midlatitude North Pacific associated with the PDO greatly influence the atmospheric transients, and hence the mean westerly jet in such a way as to reinforce the original SSTAs (Namias 1988; Gershunov and Barnett 1998). Significant SSTAs in the tropical Pacific related to ENSO mostly affect the Walker circulation and resultant Hadley circulation in the East Asian monsoon region, and hence the subtropical high in the lower and middle troposphere over the WNP (Wang et al. 2000). When an El Niño event takes place in a warm PDO epoch,

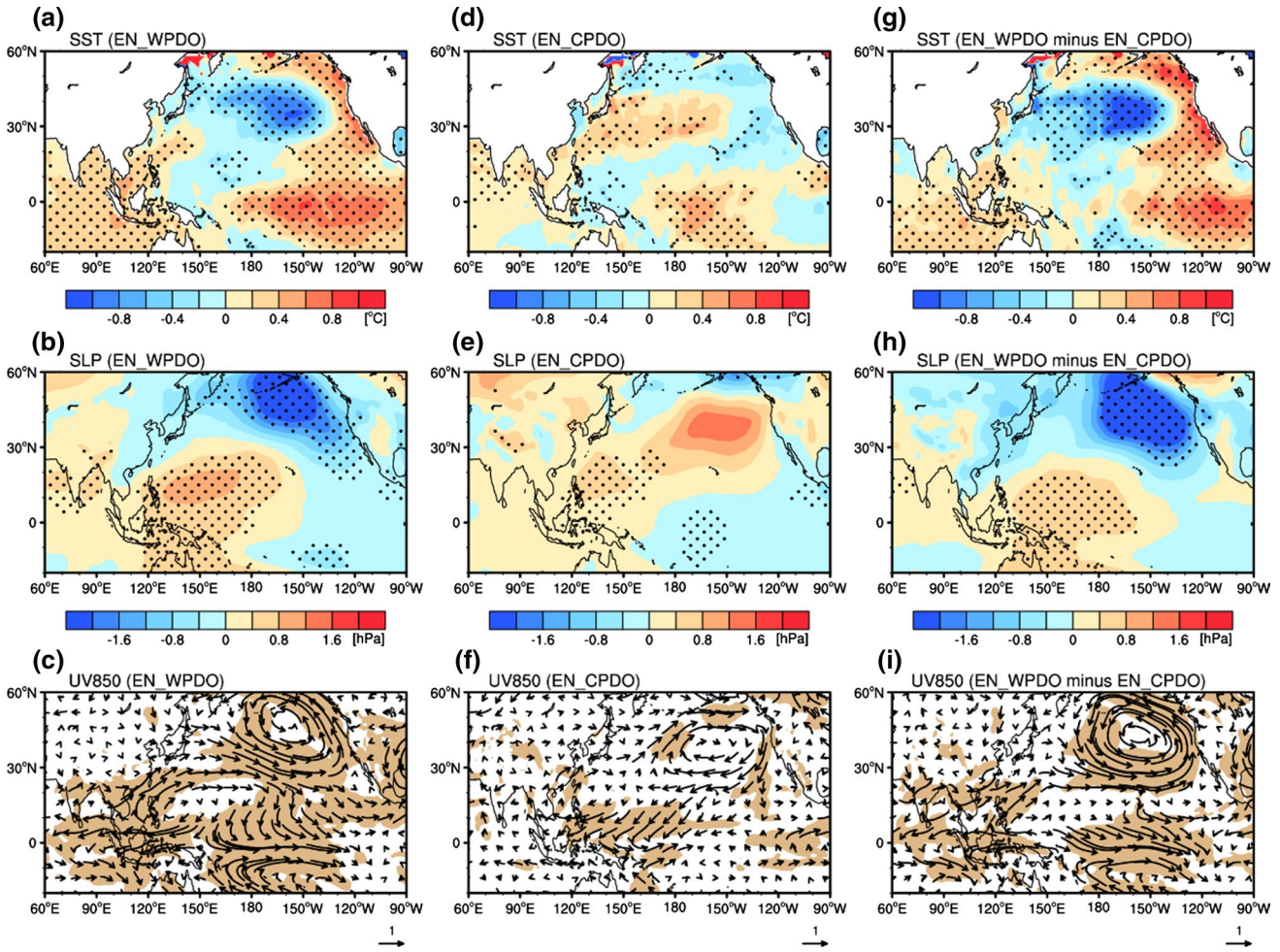

Fig. 8 Composite anomalies of spring (March–May) **a** SST (*color shading*, °C), **b** SLP (*color shading*, hPa), and **c** 850-hPa winds (*vectors*, m s^{-1}) for El Niño–warm PDO years. The *stippling* in (**a**) and (**b**) denotes statistical significance at the 95 % confidence level, while the *shading* in (**c**) indicates areas where at least one of the anomalous zonal and meridional wind components is statistically significant at the 95 % confidence level. Panels in the *middle column* (**d**–**f**) and *right column* (**g**–**i**) show corresponding anomalies for El Niño–cold PDO years and El Niño–warm PDO minus El Niño–cold PDO, respectively

the El Niño-related positive SSTAs in the equatorial eastern Pacific are strongly enhanced and the accompanying negative SSTAs in the midlatitude North Pacific are also intensified (Fig. 8a), so an El Niño–warm PDO event is characterized by both stronger positive SSTAs in the equatorial eastern Pacific and stronger negative SSTAs in the midlatitude North Pacific. This occurs because the warm PDO gives a background SSTA distribution similar to the El Niño event, meaning the SSTAs of the same sign in the equatorial Pacific and in the midlatitude North Pacific are superimposed, and are thus both further enhanced (Fig. 8a). In contrast, for El Niño–cold PDO events the El Niño-related positive SST anomalies in the equatorial eastern Pacific weaken as they are offset by the negative background SSTAs (Fig. 8d). Note, however, that weak positive anomalies are present in the central equatorial Pacific, exhibiting some features of El Niño Modoki (Ashok et al. 2007). However, the cold PDO-related positive SST anomalies still remain in the midlatitude North Pacific (Fig. 8d), for the amplitude of PDO-related SSTAs being larger than that of El Niño-related SSTAs in the North Pacific. Furthermore, the typical SSTA pattern associated with the warm PDO may be identified clearly in the difference between the El Niño–warm PDO and El Niño–cold PDO events (Fig. 8g), in which both negative SSTAs in the midlatitude North Pacific and positive SSTAs in the equatorial eastern Pacific are dominant and significant. This result indicates that the PDO indeed modifies the distribution of El Niño-related SSTAs.

Namias et al. (1988) emphasized that persistent SSTA patterns in the North Pacific are often associated with persistent atmospheric teleconnection patterns, as the atmosphere has a shorter memory than the ocean. Thus, different SSTA patterns may force different atmospheric teleconnection patterns. The composite distributions of spring SLP anomalies

show that the atmospheric response to SSTAs in an El Niño–warm PDO event is characterized by negative SLP anomalies over the Aleutian Basin and positive SLP anomalies over the WNP, indicating an enhanced Aleutian low and a simultaneously enhanced WNP subtropical high (Fig. 8b). This dipole-like SLP anomaly pattern with a northeast–southwest orientation may be a typical response of the El Niño–warm PDO combination, as suggested by Mao et al. (2011). Note the occurrence of negative SLP anomalies over the tropical eastern Pacific induced by locally positive SSTAs. As compared with the situation in Fig. 5b, the northwestern portion of the positive SLP anomalies over the WNP clearly shrinks southeastward (Fig. 8b), countered by the warm-PDO-induced negative SLP anomalies over coastal areas of East Asia (Fig. 5f). Consequently, the corresponding anomalous anticyclone over the WNP in the lower troposphere also contracts eastward in such a manner that SC is just under the influence of the anomalous southwesterlies (Fig. 8c), thus leading to above-normal rainfall over SC (Fig. 6b). Note that the anomalous cyclone over the Aleutian Basin is stronger than in El Niño (Fig. 5c) or warm PDO (Fig. 5g) events.

On the contrary, for El Niño–cold PDO events, positive SLP anomalies with larger amplitude are present over the Aleutian Basin but are not statistically significant (Fig. 8e). They extend southwestward to connect with the weak positive SLP anomalies over the WNP. Note that less significant anomalous SLP covers much larger areas including almost all coastal regions in East Asia (Fig. 8e); thus, the anomalous southwesterlies intrude farther northward into central China (Fig. 8f). However, the superposition of the El Niño-related anticyclonic anomalies with the cold PDO-related cyclonic anomalies over the WNP makes the anomalous southwesterlies much weaker and less significant over SC, resulting in less predictable SCSR (Figs. 6c, 7b). Moreover, the differences in the low-tropospheric circulation anomalies between El Niño–warm PDO and El Niño–cold PDO (Fig. 8h, i) illustrate the typical features of PDO-related circulation anomalies (Fig. 5f, g), which further indicates that the El Niño-related anomalous circulation is affected by the PDO, and that El Niño–warm PDO events are more favorable for above-normal SCSR.

The El Niño-related upper-tropospheric circulation is also modified by the PDO, which further influences the SCSR anomalies. For El Niño–warm PDO events, the SSTAs show an obvious meridional contrast, with positive anomalies in the tropical Pacific and negative anomalies over the midlatitude North Pacific (Fig. 8a), forcing a similar meridional contrast in anomalous 200-hPa geopotential height (Fig. 9a) and intensifying the upper-tropospheric westerly jets over subtropical East Asia around the southern Tibetan Plateau and over the midlatitude North Pacific (Fig. 9b). An anomalous cyclone is observed over central China, accompanied by the intensified upper-tropospheric subtropical East Asian westerly jet on its southern side (Fig. 9b), forming an upper-tropospheric divergent environment over SC, thus inducing anomalous ascending motion over the region (Fig. 9c). However, for the El Niño–cold PDO events, in response to the positive SSTAs over both the central and North Pacific (Fig. 8d), the 200-hPa geopotential height exhibits positive anomalies south of 45°N and weak negative anomalies to the north, enhancing the midlatitude westerly jet (Fig. 9e) and forcing anomalous ascending motion over central China. However, no significant anomalies in the upper-tropospheric winds occur in the subtropics. As a result, there is no significant vertical motion over SC, resulting in unpredictable SCSR. To highlight the modulating effect of PDO on the El Niño-related upper-tropospheric circulation, the differences of upper-tropospheric circulation anomalies between El Niño–warm PDO and El Niño–cold PDO are also shown (Fig. 9g, h). As a response to the warm PDO-like SSTAs (Fig. 8g), the 200-hPa geopotential height also exhibits an enhanced meridional contrast between the tropics and the midlatitudes (Fig. 9g), resulting in an enhanced subtropical East Asian westerly jet (Fig. 9h). The enhanced subtropical westerly jet further strengthens the upper-tropospheric divergence over SC and induces anomalous ascending motion over SC (Fig. 9i), contributing to the above-normal SCSR. Clearly, the composite differences of upper-tropospheric circulation between El Niño–warm PDO and El Niño–cold PDO events show some resemblance to the composite of El Niño–warm PDO events, so the El Niño-related upper-tropospheric circulation is more favorable to above-normal SCSR during warm PDO phases.

Since the modifications of La Niña-related SSTAs and circulation by the different PDO phases are similar to those of the El Niño–PDO cases, only the composite differences between La Niña–cold PDO events and La Niña–warm PDO events are shown in Fig. 10. The SSTA pattern is characterized by strong positive SSTAs in the midlatitude North Pacific and weak negative SSTA in the tropical Pacific (Fig. 10a), exhibiting some features of cold PDO events. The lower atmospheric response to the strong positive SSTAs over the North Pacific is a zonally stretched positive SLP anomaly over the North Pacific extending southwestward to the SC coastal area (Fig. 10b). Note that weak negative SLP anomalies over the western tropical Pacific may be induced by the negative tropical SSTAs (Wang et al. 2000). Thus, a meridional dipole-like circulation anomaly develops, characterized by an anomalous cyclone with a northeast–southwest orientation over the central tropical–subtropical Pacific and an anomalous elongate anticyclone stretching from SC to the midlatitude eastern North Pacific (Fig. 10c). As a result, SC is just under the divergent environment associated with the dipole-like circulation, resulting in negative SCSR anomalies (Fig. 6h). In the upper troposphere, a clear meridional contrast exists between the

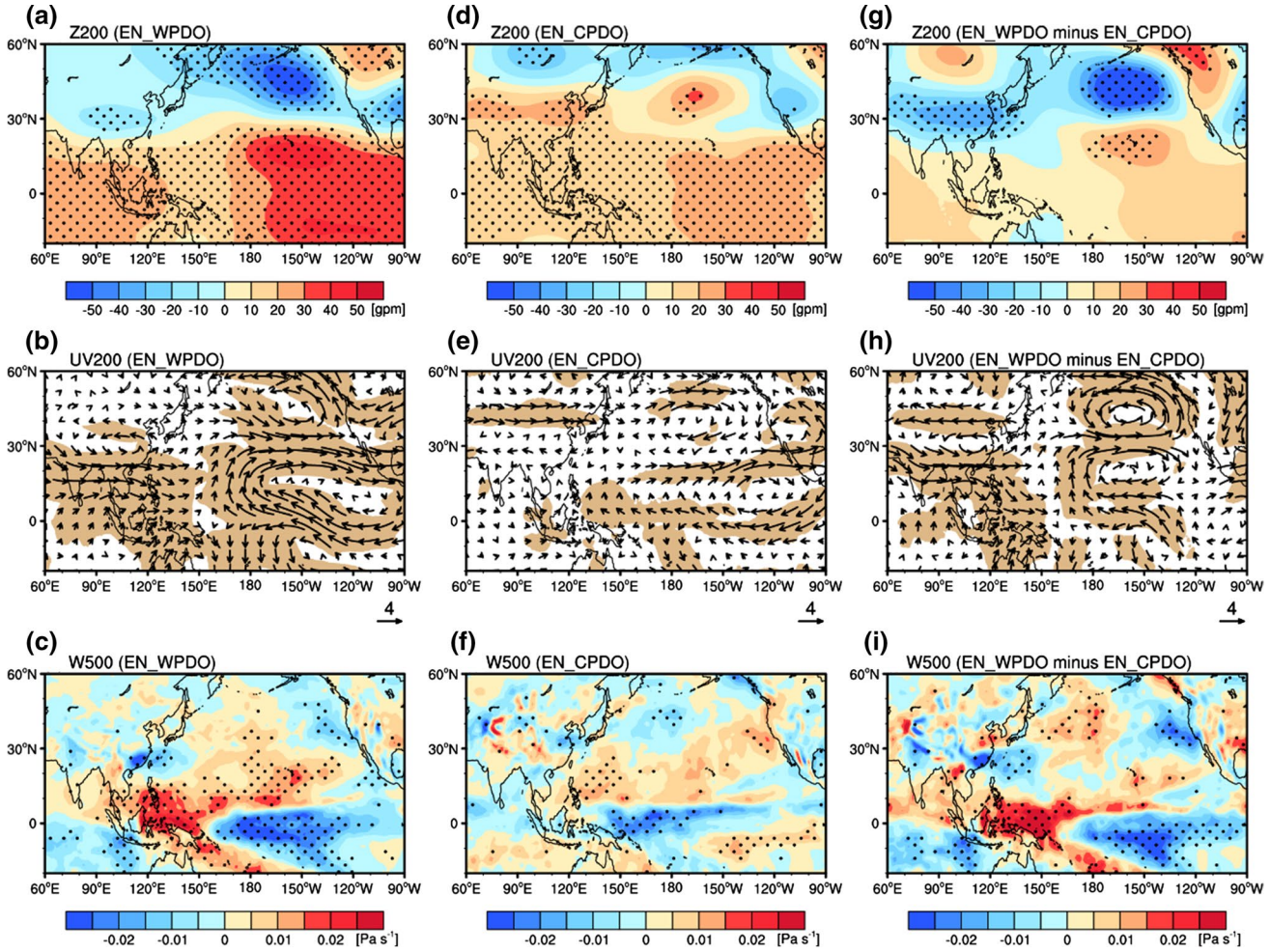

Fig. 9 Same as Fig. 8 but for (**a**), (**d**) and (**g**) 200-hPa geopotential height (*color shading*, gpm), (**b**), (**e**) and (**h**) 200-hPa winds (*vectors*, m s^{-1}), and (**c**), (**f**) and (**i**) 500-hPa vertical velocity (*color shading*, Pa s^{-1})

negative geopotential height anomalies over the tropics and positive anomalies over the midlatitudes from the Eurasian continent to the eastern North Pacific (Fig. 10d), producing anomalous easterlies along 30°N (Fig. 10f). Thus, the East Asian subtropical westerly jet over the southern Tibetan Plateau may be weakened. This weakening further reduces the divergence on the southern side of the jet entrance region (Uccellini and Kocin 1987), leading to convergent and descending anomalies over SC (Fig. 10e), and hence below-normal SCSR (Fig. 6h). Thus, the PDO also modifies the La Niña-related SSTAs and atmospheric teleconnections, and the in-phase combination (La Niña–cold PDO) is more favorable for below-normal SCSR.

5 Modulating effects in coupled models

Based on the classification method outlined in Sect. 2.3, the ENSO events in the CCSM4 historical simulation for the period 1901–2005 are categorized into four groups, with 14 El Niño–warm PDO events, 13 El Niño–cold PDO events, 14 La Niña–warm PDO events, and 16 La Niña–cold PDO events. As shown in Fig. 11, for the SC region the ENSO-related spring rainfall anomalies are considerably more significant when ENSO and PDO are in-phase, with positive anomalies during El Niño–warm PDO events (Fig. 11a) and negative anomalies during La Niña–cold PDO events (Fig. 11d). Note that corresponding to the slight northward shift of the heavy rain belt in the climatological MAM rainfall distribution simulated by the CCSM4 model (Fig. 2a), the simulated ENSO-related rainfall anomalies also extend into the Yangtze Basin, especially for the El Niño–warm PDO events. However, for out-of-phase combinations the ENSO-related rainfall anomalies show no significant wet or dry preference over SC (Fig. 11b, c). These results indicate that the modulating effect of the PDO on the ENSO–SCSR relationship is robust.

As mentioned above, the El Niño (La Niña)-related low-tropospheric anomalous anticyclone (cyclone) over

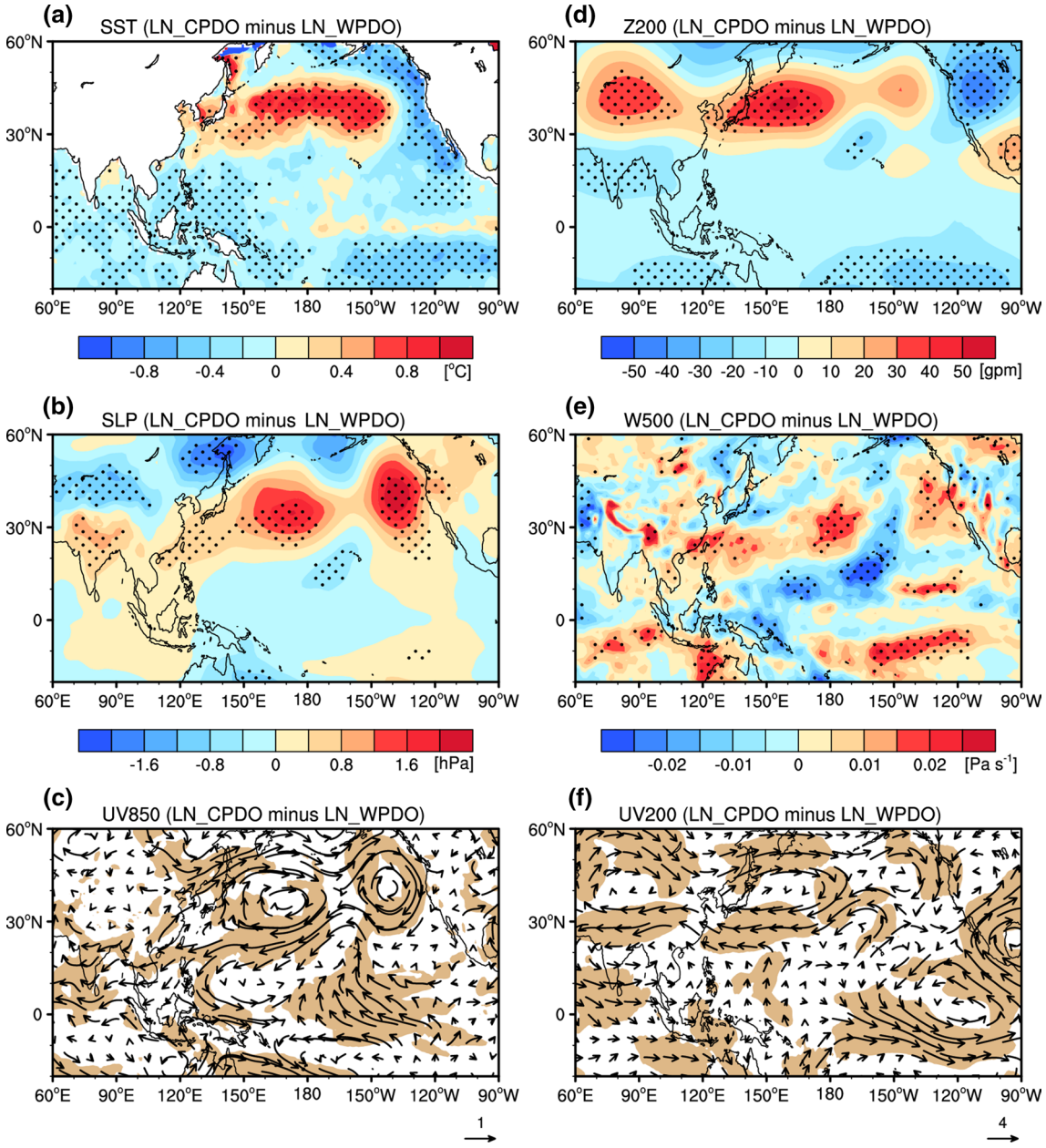

Fig. 10 Composite differences between La Niña–cold PDO events and La Niña–warm PDO events in spring (March–May) for **a** SST (*color shading*, °C), **b** SLP (*color shading*, hPa), **c** 850-hPa winds (*vectors*, m s^{-1}), **d** 200-hPa geopotential height (*color shading*, gpm), **e** 500-hPa vertical velocity (*color shading*, Pa s^{-1}), and **f** 200-hPa winds (*vectors*, m s^{-1}). The *stippling* in (**a**), (**b**), (**d**) and (**e**) denotes statistical significance at the 95 % confidence level, while the *shading* in (**c**) and (**f**) indicates areas where at least one of the anomalous zonal and meridional wind components is statistically significant at the 95 % confidence level

the WNP is the key system linking ENSO with SCSR. Figure 12a shows the composite difference of the CCSM4-simulated SSTAs for El Niño-warm PDO minus El Niño-cold PDO. The difference is characterized by features typical of a warm-PDO-related SSTA pattern, with negative anomalies in the midlatitude North Pacific and positive anomalies in the eastern equatorial Pacific and in an offshore belt along the west coast of North America and the Gulf of Alaska, strongly resembling observations (Fig. 8g). Similarly, as a response to the SSTAs an extensive anomalous anticyclone is present over the WNP accompanied by a strong anomalous cyclone centered over the North Pacific and stretching southwestwards to eastern China (Fig. 12b), inducing anomalous convergence over SC (Fig. 12c) and thus leading to above-normal SCSR (Fig. 11a). Likewise, the composite difference of the simulated SST anomalies

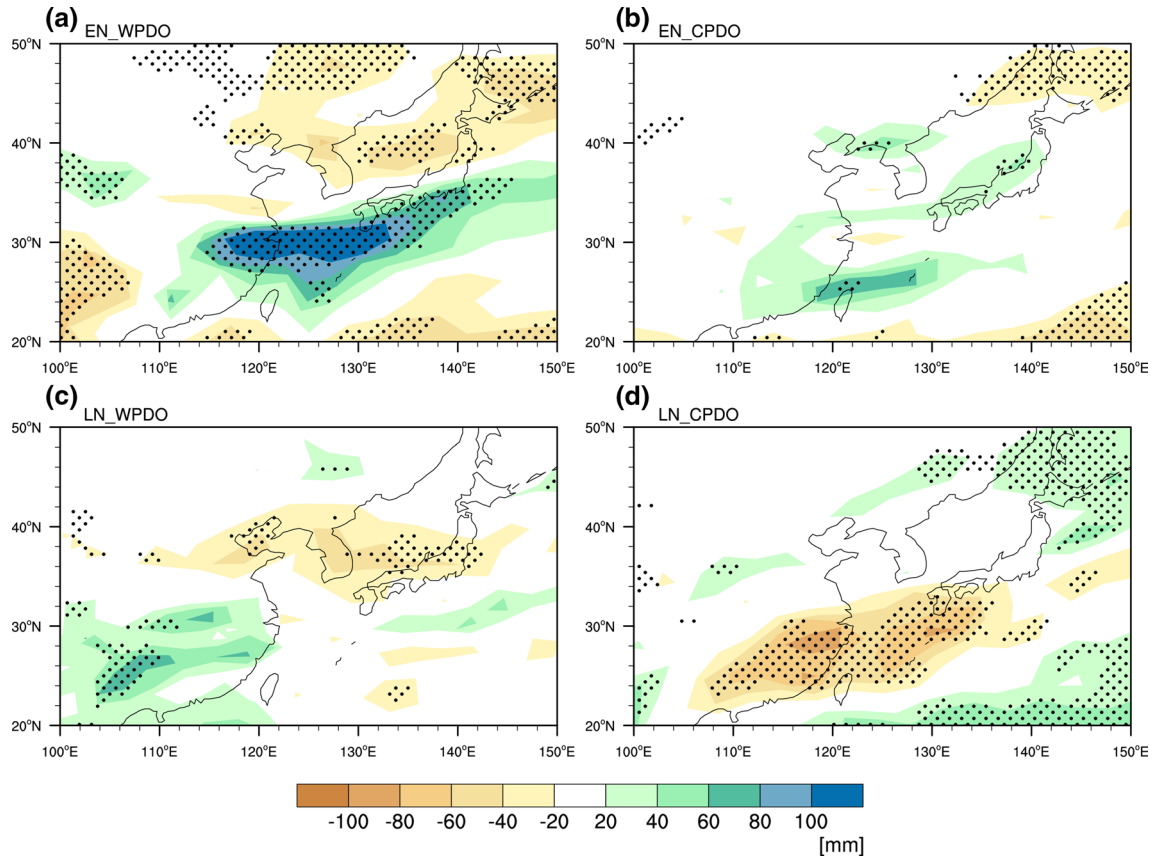

Fig. 11 Composite distributions of the CCSM4-simulated spring (March–May) detrended rainfall anomalies (*color shading*, mm) for the period 1901–2005 for **a** El Niño–warm PDO, **b** El Niño–cold PDO, **c** La Niña–warm PDO, and **d** La Niña–cold PDO. *Stippling* denotes statistical significance at the 95 % confidence level. The rainfall anomalies are calculated as departures from the seasonal mean of the base period 1901–2005

for La Niña–cold PDO minus La Niña–warm PDO is characterized by the features of a cold PDO (Fig. 12d), associated with an anomalous cyclone over the western subtropical Pacific and an anomalous anticyclone over the North Pacific (Fig. 12e), resulting in anomalous northeasterlies over SC (Fig. 12c) and leading to below-normal SCSR. This confirms that the PDO indeed modulates the strength and spatial pattern of El Niño (La Niña)-related anticyclonic (cyclonic) circulation anomalies over the WNP, which further influences the SCSR.

6 Summary and discussion

Spring rainfall over South China (SCSR) accounts for more than 35 % of the annual total and exhibits strong interannual variability, with the standard deviation exceeding 140 mm. This variability is linked to ENSO-related SSTAs in the tropical Pacific, but the positive relationship between ENSO and SCSR may not always be stable with time, and is modulated by PDO-related decadal-scale fluctuations of the North Pacific SSTAs. Therefore, the objective of the present study is to examine the physical mechanism responsible for the interdecadal modulation of the ENSO–SCSR relationship by the PDO. For this purpose, several long-term observational datasets for the period 1922–2013 were analyzed, including the Climate Research Unit gridded rainfall records CRU TS3.22, the Hadley Centre sea surface temperature (SST) dataset HadISST1.1, and the ECMWF twentieth century atmospheric reanalysis ERA–20C. The modulating mechanism thus identified was further examined with historical simulations derived from the Community Climate System Model version 4 (CCSM4).

Since ENSO is modulated by the PDO, the spring rainfall anomalies associated with an individual ENSO event on interannual timescales are actually the synthesis of the effects caused by a particular ENSO–PDO combination. When ENSO and PDO are in phase, the positive ENSO–SCSR correlation becomes much stronger, with above-normal SCSR following El Niño–warm PDO events and below-normal SCSR following La Niña–cold PDO events. The physical mechanism by which the PDO modulates the

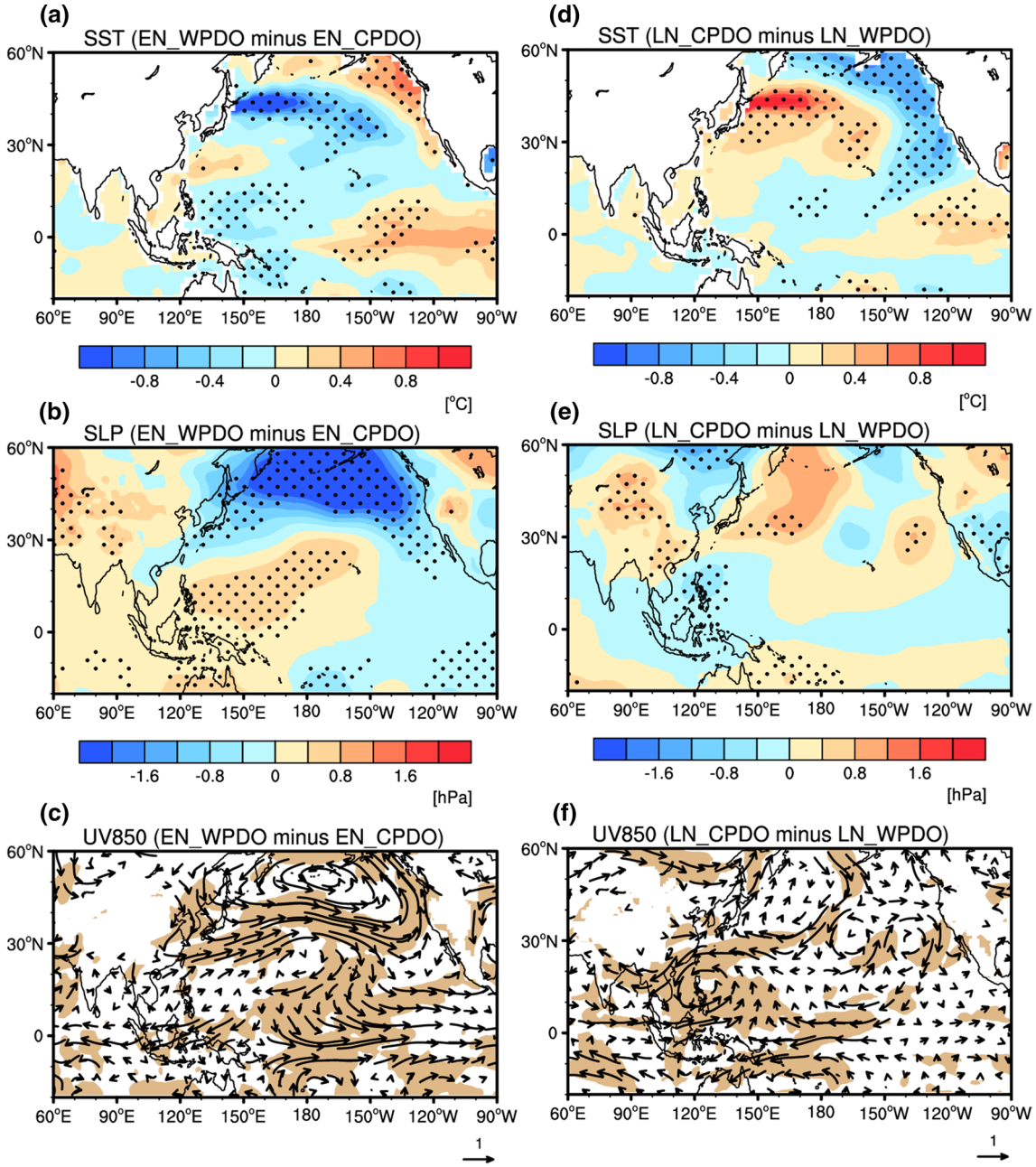

Fig. 12 Composite differences of CCSM4-simulated spring (March–May) **a** SST (*shading*, °C), **b** SLP (*shading*, hPa), and **c** 850-hPa winds (*vectors*, m s^{-1}) for El Niño–warm PDO minus El Niño–cold PDO. The *stippling* in (**a**) and (**b**) denotes statistical significance at the 95 % confidence level, while the *shading* in (**c**) indicates areas where at least one of the anomalous zonal and meridional wind components is statistically significant at the 95 % confidence level. *Right column panels* (**d**–**f**) are as (**a**–**c**), respectively, but for La Niña–cold PDO minus La Niña–warm PDO

ENSO–SCSR relationship is through the impact of variations in the subtropical anticyclone over the WNP and the upper-tropospheric westerly jet around the southern Tibetan Plateau and the midlatitude North Pacific. When an El Niño event occurs in a warm PDO epoch, the El Niño–warm PDO event is characterized by both stronger positive SSTAs in the equatorial eastern Pacific and stronger negative SSTAs in the midlatitude North Pacific, because the warm PDO itself has a similar background SSTA distribution to the El Niño event, and corresponding SSTAs with the same sign are superimposed. The atmospheric response to such an El Niño–warm PDO SSTA pattern is characterized by an enhanced Aleutian low and a simultaneously enhanced WNP subtropical anticyclone, forming a

dipole-like SLP anomaly pattern oriented northeast–southwest. Due to counteraction by the warm-PDO-induced negative SLP anomalies over coastal areas of East Asia, the corresponding anomalous anticyclone over the WNP in the lower troposphere contracts eastward so that SC is just under the influence of the anomalous southwesterlies, leading to above-normal SCSR. In the upper troposphere, the westerly jets over both subtropical East Asia around the southern Tibetan Plateau and the midlatitude North Pacific are intensified due to the enhanced meridional contrast in anomalous 200-hPa geopotential height. The intensified subtropical East Asian westerly jet produces an upper-tropospheric divergent environment on its southern side over SC, driving anomalous ascending motion over SC, and hence above-normal SCSR. A similar situation occurs when a La Niña event occurs in a cold PDO epoch, except that the La Niña–cold PDO event leads to below-normal SCSR. Because both enhanced negative SSTAs in the equatorial eastern Pacific and enhanced positive SSTAs in the midlatitude North Pacific force an anomalous cyclone over the NWP along with a weakened westerly jet over East Asia, the result is significant descending motion over SC.

In contrast, when ENSO and the PDO are out-of-phase, the ENSO–SCSR relationship is weakened and less significant. For El Niño–cold PDO events, the El Niño-related positive SST anomalies in the equatorial eastern Pacific become much weaker due to counteraction by the negative PDO background SSTAs, exhibiting some of the features of El Niño Modoki. Although positive SLP anomalies with larger amplitude are present over the Aleutian Basin, they are not statistically significant. These anomalies extend southwestward to connect with the weak positive SLP anomalies over the WNP. Because the El Niño-induced anticyclonic anomalies are to some extent counteracted by the cold PDO-induced cyclonic anomalies over the WNP, the anomalous southwesterlies become much weaker and insignificant over SC. In terms of the upper-tropospheric winds, there are no significant anomalies in the subtropics, so no significant vertical motion exists over SC, leading SCSR to become unpredictable. Likewise, the La Niña–warm PDO events also lead to unpredictable SCSR, without any anomalous wet or dry preference of SCSR.

The CCSM4 simulations perform well in reproducing the SSTAs and low-tropospheric circulation differences between El Niño–warm PDO events and El Niño–cold PDO events. There are positive SSTAs in the eastern Pacific and negative SSTAs in the midlatitude North Pacific, which confirms that the El Niño-related SSTAs are enhanced (weakened) during warm (cold) PDO phases. Furthermore, the extensive anomalous anticyclone over the western subtropical Pacific is also captured well by CCSM4, as is the anomalous zonally stretched cyclone over the North Pacific and eastern China, although their intensities are weaker than those in the observations. Thus, the anticyclone over the WNP and the cyclone over the midlatitude North Pacific are actually the key systems through which the PDO modulates the ENSO-related SCSR. The simulated differences between La Niña–cold PDO events and La Niña–warm PDO also confirm the modulating process derived from the observations.

This study demonstrated that the PDO could modify the relationship between ENSO and seasonal-mean spring rainfall over SC. However, the rainfall distribution in any one year or season is made up of a series of low-frequency sequences of rainy periods ("active" periods) with intervening dry periods (monsoon "breaks") each lasting 10–30 days (Webster and Hoyos 2004). SCSR also possesses a significant 10–20-day intraseasonal variability for most springs (Pan et al. 2013), thus such intraseasonal behaviors of SCSR may be influenced by different ENSO-PDO combinations, with their influences to happen similar to the situations of the ENSO events on the intraseasonal variability of the EASM in different PDO phases, as was suggested by Yun et al. (2010) and Lee et al. (2010). Thus, an investigation of how ENSO affects the intraseasonal SCSR under different PDO backgrounds could be helpful to understand the interannual variability of seasonal-mean SCSR and to improve its predictability, which will be explored in the future. Furthermore, besides the SSTAs in the Pacific, the SSTAs in the Indian Ocean have recently been found to have a large impact on East Asian climate variability (Watanabe and Jin 2003; Yang et al. 2007; Ding et al. 2010). As suggested by Chen et al. (2013a), the decadal change of SSTs in the South Indian Ocean around the mid-1970s may also modulate the relationship between SC winter–spring rainfall and ENSO. Thus, to further explore the predictability of SCSR, the influence of SSTAs in the Indian Ocean in association with the PDO modulation of the ENSO–SCSR relationship will be the subject of further research.

Acknowledgments The authors thank the two anonymous reviewers for their constructive suggestions. This research was jointly supported by the National Basic Research Program of China (2014CB953902, 2012CB955202, and 2012CB417203), the Priority Research Program of the Chinese Academy of Sciences (XDA11010402), and the Natural Science Foundation of China (41175059, 41375087, and 91537103).

References

Ashok K, Behera SK, Rao SA, Weng HY, Yamagata T (2007) El Niño Modoki and its possible teleconnection. J Geophys Res 112:C11007. doi:10.1029/2006jc003798

Chan JCL, Zhou W (2005) PDO, ENSO and the early summer monsoon rainfall over South China. Geophys Res Lett 32:L08810. doi:10.1029/2004gl022015

Chen J, Wen Z, Wu R, Chen Z, Zhao P (2013a) Interdecadal changes in the relationship between southern China winter–spring precipitation and ENSO. Clim Dyn 43:1327–1338

Chen W, Feng J, Wu RG (2013b) Roles of ENSO in the link of the East Asian winter monsoon to the following summer monsoon. J Clim 26:622–635

Compo GP et al (2011) The twentieth century reanalysis project. Q J R Meteorol Soc 137:1–28

DeFlorio MJ, Pierce DW, Cayan DR, Miller AJ (2013) Western U.S. extreme precipitation events and their relation to ENSO and PDO in CCSM4. J Clim 26:4231–4243

Deng LP, Wang QQ (2002) On the relationship between precipitation anomalies in the first raining season (April–June) in southern China and SST over offshore waters in China. J Trop Meteorol 18:45–55 **(in Chinese)**

Ding YH (2004) Seasonal March of the East-Asian summer monsoon. In: Chang CP (ed) East Asian Monsoon. Mainland Press, Singapore, pp 3–53

Ding RQ, Ha K-J, Li JP (2010) Interdecadal shift in the relationship between the East Asian summer monsoon and the tropical Indian Ocean. Clim Dyn 34:1059–1071

Efron B (1982) The jackknife, the bootstrap and other resampling plans. Capital City Press, Montpelier, pp 27–36

Feng J, Li JP (2011) Influence of El Niño Modoki on spring rainfall over South China. J Geophys Res 116:D13102. doi:10.1029/2010jd015160

Feng J, Wang L, Chen W (2014) How does the East Asian Summer Monsoon behave in the decaying phase of El Niño during different PDO phases? J Clim 27:2682–2698

Gao H, Wang YG, He JH (2006) Weakening significance of ENSO as a predictor of summer precipitation in China. Geophys Res Lett 33:L09807. doi:10.1029/2005gl025511

Gershunov A, Barnett TP (1998) Interdecadal modulation of ENSO teleconnections. Bull Am Meteorol Soc 79:2715–2725

Gong DY, Wang SW (1998) Impact of ENSO on the seasonal rainfall in China. J Nat Disasters 7:44–52 **(in Chinese)**

Ha K-J, Heo K-Y, Lee S-S, Yun K-S, Jhun J-G (2012) Variability in the East Asian Monsoon: a review. Meteorol Appl 19:200–215

Harris I, Jones PD, Osborn TJ, Lister DH (2014) Updated high-resolution grids of monthly climatic observations-the CRU TS3.10 Dataset. Int J Climatol 34:623–642

Huang RH, Wu YF (1989) The influence of ENSO on the summer climate change in China and its mechanism. Adv Atmos Sci 6:21–32

Karori MA, Li JP, Jin FF (2013) The asymmetric influence of the two types of El Niño and La Niña on Summer Rainfall over Southeast China. J Clim 26:4567–4582

Kim JW, Yeh SW, Chang EC (2014) Combined effect of El Niño-Southern Oscillation and Pacific Decadal Oscillation on the East Asian winter monsoon. Clim Dyn 42:957–971

Krishnamurthy L, Krishnamurthy V (2014) Influence of PDO on South Asian summer monsoon and monsoon-ENSO relation. Clim Dyn 42:2397–2410

Lau KM, Li MT (1984) The Monsoon of East-Asia and its global associations—a survey. Bull Am Meteorol Soc 65:114–125

Lee S-S, Vinayachandran PN, Ha K-J, Jhun J-G (2010) Shift of peak in summer monsoon rainfall over Korea and its association with ENSO. J Geophys Res 115:D02111. doi:10.1029/2009JD011717

Lee S-S, Seo Y-W, Ha K-J, Jhun J-G (2013) Impact of the western North Pacific subtropical high on the East Asian Monsoon precipitation and the Indian Ocean precipitation in the boreal summertime. Asia-Pac J Atmos Sci 49:171–182

Li J, Yu RC, Yuan WH, Chen HM, Sun W, Zhang Y (2015) Precipitation over East Asia simulated by NCAR CAM5 at different horizontal resolutions. J Adv Model Earth Syst 7:774–790

Linho LH, Huang XL, Lau NC (2008) Winter-to-spring transition in East Asia: a planetary-scale perspective of the South China spring rain onset. J Clim 21:3081–3096

Mantua NJ, Hare SR, Zhang Y, Wallace JM, Francis RC (1997) A Pacific interdecadal climate oscillation with impacts on salmon production. Bull Am Meteorol Soc 78:1069–1079

Mao JY, Chan JCL, Wu GX (2004) Relationship between the onset of the South China Sea summer monsoon and the structure of the Asian subtropical anticyclone. J Meteorol Soc Jpn 82:845–859

Mao JY, Chan JCL, Wu GX (2011) Interannual variations of early summer monsoon rainfall over South China under different PDO backgrounds. Int J Climatol 31:847–862

Namias J, Yuan XJ, Cayan DR (1988) Persistence of North Pacific Sea surface temperature and atmospheric flow patterns. J Clim 1:682–703

Pan WJ, Mao JY, Wu GX (2013) Characteristics and mechanism of the 10–20-day oscillation of spring rainfall over southern China. J Clim 26:5072–5087

Qiang XM, Yang XQ (2013) Relationship between the first rainy season precipitation anomaly in South China and the sea surface temperature anomaly in the Pacific. Chin J Geophys 56:2583–2598 **(in Chinese)**

Rayner NA et al (2003) Global analyses of sea surface temperature, sea ice, and night marine air temperature since the late nineteenth century. J Geophys Res 108(D14):4407. doi:10.1029/2002JD002670

Shao TH, Zhang YC (2012) Influence of winter North Atlantic Oscillation on spring precipitation in China. Plateau Meteorol 31:1225–1233 **(in Chinese)**

Sperber K et al (2013) The Asian summer monsoon: an intercomparison of CMIP5 vs. CMIP3 simulations of the late 20th century. Clim Dyn 41:2711–2744

Stickler A et al (2014) ERA-CLIM historical surface and upper-air data for future reanalyses. Bull Am Meteorol Soc 95:1419–1430

Tao SY, Chen LX (1987) A review of recent research on the East Asian summer monsoon in China. In: Chang CP, Krishnamurti TN (eds) Monsoon meteorology. Oxford University Press, London, pp 60–92

Tao SY, Zhang QY (1998) Response of the Asian winter and summer monsoon to ENSO events. Sci Atmos Sin 22:399–407 **(in Chinese)**

Taylor KE, Stouffer RJ, Meehl FA (2012) An overview of CMIP5 and the experiment design. Bull Am Meteorol Soc 93:485–498

Uccellini LW, Kocin PJ (1987) The interaction of jet streak circulations during heavy snow events along the east coast of the United States. Weather Forecast 2:289–308

Wan RJ, Wu GX (2009) Temporal and spatial distributions of the spring persistent rains over Southeastern China. Acta Meteorol Sin 23:598–608

Wang B, Wu RG, Fu XH (2000) Pacific-East Asian teleconnection: how does ENSO affect East Asian climate? J Clim 13:1517–1536

Wang B, Yang J, Zhou TJ (2008) Interdecadal changes in the major modes of Asian-Australian monsoon variability: strengthening relationship with ENSO since the late 1970s. J Clim 21:1771–1789

Wang SS, Huang JP, He YL, Guan YP (2014) Combined effects of the Pacific Decadal Oscillation and El Niño–Southern Oscillation on global land dry–wet changes. Sci Rep 4:6651. doi:10.1038/Srep06651

Watanabe M, Jin FF (2003) A moist linear baroclinic model: coupled dynamical-convective response to El Niño. J Clim 16:1121–1139

Webster PJ, Hoyos C (2004) Prediction of monsoon rainfall and river discharge on 15–30-day time scales. Bull Am Meteorol Soc 85:1746–1765

Wu RG, Kirtman BP (2007) Observed relationship of spring and summer East Asian rainfall with winter and spring Eurasian snow. J Clim 20:1285–1304

Wu RG, Hu ZZ, Kirtman BP (2003) Evolution of ENSO-related rainfall anomalies in East Asia. J Clim 16:3742–3758

Yang FL, Lau KM (2004) Trend and variability of China precipitation in spring and summer: linkage to sea-surface temperatures. Int J Climatol 24:1625–1644

Yang JL, Liu QY, Xie SP, Liu ZY, Wu LX (2007) Impact of the Indian Ocean SST basin mode on the Asian summer monsoon. Geophys Res Lett 34:L02708. doi:10.1029/2006gl028571

Yoon J, Yeh SW (2010) Influence of the Pacific Decadal Oscillation on the relationship between El Niño and the Northeast Asian Summer Monsoon. J Clim 23:4525–4537

Yu B, Zwiers FW (2007) The impact of combined ENSO and PDO on the PNA climate: a 1,000-year climate modeling study. Clim Dyn 29:837–851

Yun K-S, Seo K-H, Ha K-J (2010) Interdecadal change in the relationship between ENSO and the intraseasonal oscillation in East Asia. J Clim 23:3599–3612

Zheng F, Li JP (2012) Impact of preceding boreal winter southern hemisphere annular mode on spring precipitation over South China and related mechanism. Chin J Geophys 55:3542–3557 **(in Chinese)**

Zheng F, Li JP, Wang L, Xie F, Li XF (2015) Cross-seasonal influence of the December–February southern hemisphere annular mode on March–May meridional circulation and precipitation. J Clim. doi:10.1175/jcli-d-14-00515.1

Zhou LT, Wu RG (2010) Respective impacts of the East Asian winter monsoon and ENSO on winter rainfall in China. J Geophys Res 115:D02107. doi:10.1029/2009jd012502

Zhou LT, Tam CY, Zhou W, Chan JCL (2010) Influence of South China Sea SST and the ENSO on winter rainfall over South China. Adv Atmos Sci 27:832–844

Zhu YM, Yang XQ (2003) Relationships between Pacific Decadal Oscillation (PDO) and climate variabilities in China. Acta Meteorol Sin 61:641–654 **(in Chinese)**